Article

Effects of Cracks and Geometric Parameters on the Flow in Shale

Li Lu, Yingjun Li,* and Xuhui Zhang

Cite This: *ACS Omega* 2021, 6, 4619−4629

Read Online

ACCESS | Metrics & More | Article Recommendations

ABSTRACT: In recent years, shale oil/gas has become increasingly important in global energy. The natural pores of shale are mainly of micro−nano sizes and have the cross-scale characteristics, which makes the traditional method difficult and impractical in studying the seepage of shale. In order to obtain the characteristics of seepage of the crack-pore-throat system, the lattice Boltzmann method and dimensional analysis were used to study the seepage in an idealized crack-pore network. The influences of the geometric factors, including crack location, crack opening, and interval between two vertical neighbor throats and boundary conditions on the seepage were studied. The results show that the slip boundary conditions enhance the seepage rate. The enhancement with slip coefficients is nonuniform. The total flux is nearly equal when the crack is near either the inlet or outlet, but larger than that when the crack is located in the middle of the model. The flux ratio between the main throats when the crack is located near the outlet is the greatest. When the crack is near the outlet, the water channel is the largest possible while it is not easy to form when the crack is in the middle. With increase in the opening ratio of the crack-to-throat, the total flow of the system increases. The increase degree decreases with the increasing opening ratio. When the opening ratio is greater than 9, the increase in flux becomes very small. If the crack-pore-throat system is very uniform or even symmetric, the flow rate in the vertical throat/crack is very small. Hence, it is not beneficial to the gas/oil production and gas/oil displacement.
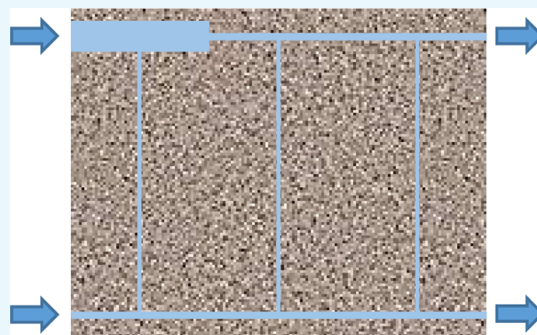
1. INTRODUCTION

The dwindling of conventional reservoirs means that the current developments in oil and gas production have to spread to unconventional reservoirs, such as tight gas, tight oil, shale gas, and shale oil reserves, in order to meet the growing demand.[1] Fluid flow in unconventional reservoirs is affected by many factors, such as pore structure characteristics, matrix wettability, organic matter, and so forth.[2,3] The most noteworthy feature of unconventional reservoirs is the low to ultralow permeability due to the very small pore-throat system, which severely influences the fluid flow, adsorption/desorption, and so forth.[4,5] Studies have shown that hydraulic fracturing can improve the connectivity and complexity of natural fractures.[6,7] That is why massive hydraulic fracturing becomes the most important technique to improve oil and gas recovery in low-permeability reservoirs.[8,9] In addition, studies have shown that in the spontaneous imbibition process of shale, small fractures induced by clay expansion effects will significantly affect its permeability.[10,11] The cracks, either natural or hydraulic, form the main flow channel, while the pore-throat system has the auxiliary function of enhancing the gas/oil product in unconventional reservoirs.

The existence of cracks increases the complexity and heterogeneity of the unconventional reservoirs. On one hand, it can enhance gas/oil recovery if the cracks are distributed properly and so the flow is relatively uniform and has the largest influence range; on the other hand, it will reduce the gas/oil recovery greatly if the cracks promote the occurrence of the water channel.[12] The flow simulation on unconventional oil/gas reservoir has been carried out in recent years. Because of the multiscale character of the seepage system, the flow in unconventional reservoir ranges from continuous to free-molecule flow. Traditional theories (such as Darcy law) must be modified by considering the Knudsen effects to describe the seepage characteristics.[13] Most previous studies were focused on the distribution of velocity, effects of boundary conditions (slip or not) in a throat or a crack. Percolation theory has been used to study the connection in tight reservoirs.[14] A network model was used to analyze the permeability and displacement effects but does not concern the flow details.[15] In brief, few studies are carried out to investigate the detail flow characteristics in the unconventional reservoirs with nonuniformly distributed seepage system. A large part of the reason lies in the lack of suitable methods.

Lattice Boltzmann method (LBM), a method based on the Boltzmann collision equation in statistical physics, has been rapidly developed over the past three decades and has been widely used in many fields. As a kind of mesoscopic method, LBM has a strong theoretical background and some numerical advantages. It can describe nonequilibrium dynamics including interfacial dynamics and complex boundaries.[16] In addition, LBM can be used to simulate the flow in different scales (different Knudsen numbers) by the same equations. So LBM is a strong tool for studying the multiscale phenomena. Because of the above advantages, LBM is an ideal method for simulating the seepage in shale. In recent years, LBM has been widely used in the studies of microscale seepage. Fathi et al.[17,18] studied the flow of gas in nanoscale monopores and kerogen. Ning et al.[19,20] simulated the gas flow in shale reservoirs and analyzed the microscale effects. The effects of adsorption and desorption processes on shale gas production processes were also studied. Benamram et al.[21] used LBM to simulate shale reservoirs after artificial fracturing. Wang et al.[22] proposed a gas flow under high Knudsen number for simulating shale gas reservoirs. Moghaddam and Jamiolah-mady.[23] studied the slip flow in a single channel. The effects of boundary conditions were discussed. Li et al.[24] investigated the flow characteristic of shale gas in sudden and gradual contraction channels.

From the above viewpoint, most previous investigations are based on simple geometries such as a tube or a throat. Few studies have been carried out on the characteristics of flow, especially nonuniform flow in a pore-throat-crack system. These characteristics directly determine the oil/gas production and displacement efficiency. In this study, LBM was used to simulate the fluid flow in the shale rock to study the influences of the crack and the geometric parameters. Dimensional analysis was first processed to obtain the main factors and simplify the problem. Then, the influences of geometric parameters on the flow characteristics were studied. The slip and nonslip boundary conditions with different rebound coefficients were simulated so as to investigate the effects of boundary conditions.

2. DESCRIPTION OF THE PROBLEM

The model considered in the following simulation is a rectangle zone. Some horizontal and vertical distributed throats form the main passageway of fluid flow. The model is assumed to be symmetric laterally, so only the lower half part is simulated. Two rows of horizontal throats are connected by three vertical throats. Each row of horizontal throats consisted of four throats. The intersection of any two throats or crack and throat is the pore. The sizes of the two horizontal throats are equal. A crack extends horizontally and is set at the inlet, middle, and outlet, respectively, to study the effects of locations. The fluid is injected from the left side and flows out of the right side. The flow on the upper and lower sides are forbidden. Only single-phase fluid is considered, so there is no capillary force. The influences of gravity can be neglected in small pore/throat/crack. The flux and pressure are investigated under different conditions.

The geometric arrangement of the pore throats and crack is shown in Figure 1. The gray part is the solid skeleton, the white fine lines (throats) and thick lines (cracks) form the network of fluid flow. The two rows of throats (named as the main throats m_1 and m_2, respectively) extending in the horizontal direction are named as main throats. The three
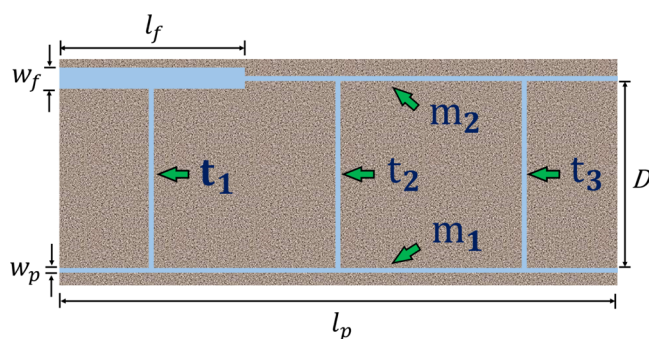

Figure 1. Schematic of the pore network. The gray part is a solid skeleton, fine blue lines are throats, and the thick blue is a crack. The intersection points between any two throats or between any throat and the crack are pores. The horizontal throats are named as main throats. The vertical throats are named as traffic throats in the following text.

throats (t_1, t_2, and t_3) extending in the vertical direction are named as traffic throats. The intersection points between any two throats or between any throat and the crack are pores. The fluid flows into the main throat at the left side under the pressure difference and is out of the network from the right side (named outlet end). The traffic throats are set with equal interval. The length of the crack is set to be one-third of that of any row main throat.

2.1. Dimensional Analysis. Dimensional analysis is a widely used analytical method. This method uses carefully selected dimensionless numbers to replace the variables in the original problem to study the influencing factors of similar problems.[7] This paper introduces this analysis method to study the influence of the geometric parameters of fractures and pore networks on fluid flow in pore structures of different scales. According to the description of the above section, the factors of the problem are as follows.

2.1.1. Geometric Factors. Throat opening w_p, crack opening w_f, interval between the two rows of horizontal throats (main throats) D, total length of each row of horizontal throat l_p, and crack's length l_f;

2.1.2. Factors of Fluid. Hydrodynamic viscosity μ, density of water ρ, and molecule-free-path λ;

2.1.3. Factors of Loading. Pressure difference between outlet and inlet is Δp;

2.1.4. Dependent Variables. Flux out of the two throats at the outlet Q_{up}, Q_{down}, pressure p, velocity v.

Then, the dependent variables can be expressed as the function of the other factors

$$\left\{ \begin{array}{c} Q_{up} \\ Q_{down} \\ p \\ V \end{array} \right\} = f(w_p, w_f, D, l_p, l_f, \mu, \rho, \Delta p, \lambda) \quad (1)$$

Let w_p, μ, and ρ to normalize the other factors

$$
\begin{cases}
\dfrac{\rho Q_{up}}{w_p \mu} \\[2mm]
\dfrac{\rho Q_{down}}{w_p \mu} \\[2mm]
\dfrac{p \rho w_p^2}{\mu^2} \\[2mm]
\dfrac{V \rho w_p}{\mu}
\end{cases}
= f\left(\dfrac{w_f}{w_p}, \ \dfrac{D}{w_p}, \ \dfrac{l_p}{w_p}, \ \dfrac{l_f}{l_p}, \ \dfrac{\rho \Delta p w_p^2}{\mu^2}, \ \dfrac{\lambda}{w_p} \right) \tag{2}
$$

It can be seen that there are six dimensionless controlling parameters in this problem. Five are dimensionless characteristic scale and one is pressure difference. The pressure difference ΔP and the horizontal pore length are both set to be constant, for example, the pressure gradient is constant, considering the aim of this study is to investigate the effects of the crack and geometric parameters. The parameter l_p/w_p is very small. It is assumed that $l_f = l_p/3$ in the previous section. Considering the aim of this paper, the effects of geometric parameters are investigated, and the Knudsen number (λ/w_p) affects only the value of the velocity but not the distribution, the Knudsen number is fixed to a value in the range of slip zone in the simulation. Therefore, the dimensionless controlling parameters considered in the numerical simulation are w_f/w_p and D/w_p (namely, the opening ratio of throat-to-crack and dimensionless interval between the two main throats).

If the numerical unit of each parameter in the following text is not marked, it is a dimensionless quantity.

2.2. Computational Method.

2.2.1. Lattice Boltzmann Model.

LBM is originated from lattice gas automata. It can also be directly derived from the continuous Boltzmann equation.[24] Lattice Boltzmann equation (LBE), containing two terms: collision and streaming, is difficult to be solved directly because of the complex multivariable integral in the collision term until several collision operators[25,26] have been proposed such as multiple relaxation time model.[27]

A collision term in LBE indicates that the particles reaching a lattice node collide and change their velocity direction by the collision operator; and a streaming term indicates that each fluid particle moves to the neighbor lattice node along its velocity's direction. The general form of LBE includes a lattice pattern, a local equilibrium distribution function apart from LBE itself.

A Bhatnagar–Grook–Krook (BGK) collision operator, one of the most efficient operators,[28,29] is derived on the basis of linearization of the collision operator around the equilibrium state, neglecting the higher-order terms. Qian[30] presented an extensively popular 2D LBM model where a single particle mass has eight directions and three magnitudes. This model is known as D2Q9, indicating 2D and nine velocities. The magnitude of velocities is defined in eq 4.

In this work, the model presented by Leclaire et al.[31] is adopted to simulate the flow in a pore-throat-crack network. The two steps are introduced simply in the following

Step 1: Collision

$$
f_\alpha(\vec{r} + \vec{e}_\alpha \delta_t, \ t + \delta_t) - f_\alpha(\vec{r}, \ t)
$$
$$
= -\frac{1}{\tau}[f_\alpha(\vec{r}, \ t) - f_\alpha^{eq}(\vec{r}, \ t)] \tag{3}
$$

where f_α is the distribution function, τ is the relaxation time and is set as 1.035 in the following computation, r is the coordinates, t is the time, f_α^{eq} is the discrete equilibrium distribution function, and $\vec{e}_\alpha$ is the discrete velocity and equals

$$
\vec{e}_\alpha = \begin{cases}
(0,0) & \alpha = 0 \\[1mm]
c\left(\cos\left[(\alpha - 1)\dfrac{\pi}{2}\right], \ \sin\left[(\alpha - 1)\dfrac{\pi}{2}\right] \right) \\
\qquad \alpha = 1,2,3,4 \\[1mm]
\sqrt{2}\,c\left(\cos\left[(2\alpha - 1)\dfrac{\pi}{4}\right], \ \sin\left[(2\alpha - 1)\dfrac{\pi}{4}\right] \right) \\
\qquad \alpha = 5,6,7,8
\end{cases} \tag{4}
$$

where $c = \delta_x/\delta_t$, δ_x, and δ_t are the size step and time step for each lattice. Let $\delta_x = \delta_y = \delta_t = 1$ in this paper.

f_α^{eq} can be determined by the following equation

$$
f_\alpha^{eq}(x) = \omega_\alpha \rho \left[1 + 3\frac{\vec{e}_\alpha \cdot \vec{U}}{c^2} + \frac{9}{2}\frac{(\vec{e}_\alpha \cdot \vec{U})^2}{c^4} - \frac{3}{2}\frac{\vec{U}^2}{c^2} \right] \tag{5}
$$

where ρ the density, $\vec{U}$ is the velocity, ω_α is the weight coefficient, and the values are given as follows

$$
\omega_\alpha = \begin{cases}
4/9, & \alpha = 0 \\
1/9, & \alpha = 1,2,3,4 \\
1/36, & \alpha = 5,6,7,8
\end{cases} \tag{6}
$$

The macroscopic density ρ is related with the distribution function of particle density, f_α, by the following equation

$$
\rho = \sum_{\alpha=0}^{8} f_\alpha \tag{7}
$$

The macroscopic flow velocity can be obtained by

$$
\vec{U} = \frac{1}{\rho} \sum_{\alpha=0}^{8} f_\alpha \vec{e}_\alpha \tag{8}
$$

The kinematic viscosity of the fluid is $\nu = (\tau - 0.5)RT$, R is the ideal gas constant, T is the temperature, $RT = 1/3$ in D2Q9, and the macroscopic pressure is given by $p = \rho c_s^2$.

2.2.2. Boundary Conditions.

Generally, the rebound format is often used in LBM to simulate a nonslip boundary. The accuracy of the standard rebound format is only of first order, but it is of second order at the inner nodes, so a half-step bounce format (see Figure 2), proved to have second-order accuracy,[32] is adopted. This format takes a virtual boundary as the calculation boundary which is half a step from the physical
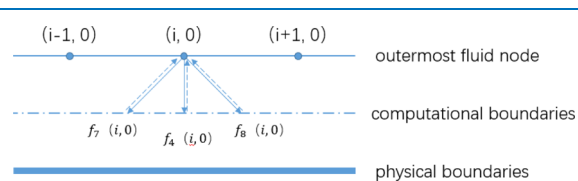
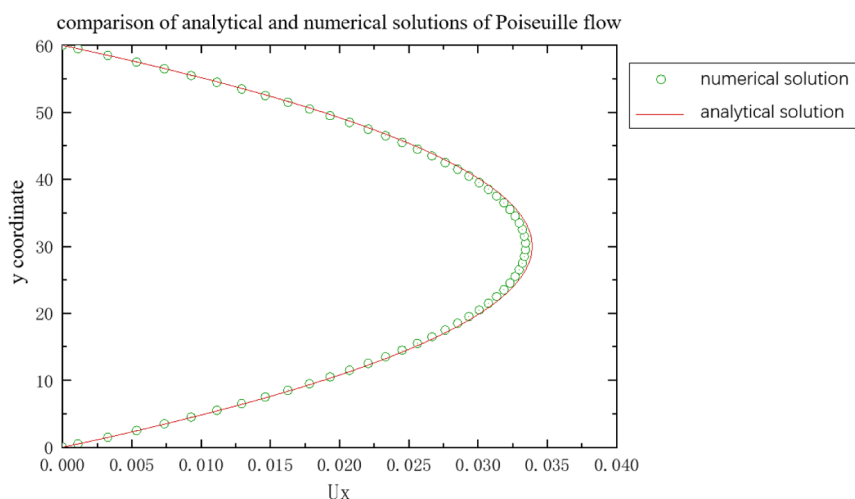**Figure 2.** Schematic diagram of the boundary rebound format.

Figure 3. Comparison of numerical solution and analytical solution for two-dimensional Poiseuille flow.

boundary. The unknown distribution functions on the boundary nodes are determined by

$$f_2(i, 0) = f_4(i, 0)$$
$$f_5(i, 0) = f_7(i, 0)$$
$$f_6(i, 0) = f_8(i, 0) \tag{9}$$

When the wall is absolutely smooth and so there is no exchange of intermolecular momentum between the fluid and the boundary, the specular reflection format is usually used to simulate this type of free-slip boundary. The unknown distribution functions on the boundary nodes are obtained by

$$f_2(i, 0) = f_4(i, 0)$$
$$f_5(i, 0) = f_8(i - 1,0)$$
$$f_6(i, 0) = f_7(i + 1,0) \tag{10}$$

However, both the rebound format and the specular reflection format cannot be simply used to describe the interaction between the fluid and the boundary in micro–nanoscale channels. The reason is that the slip effects become more and more obvious with the increase of Knudsen number. The bounce-back and specular-reflection schemes (BSR) proposed by Succi are adopted in the following simulation. At higher Knudsen numbers, this scheme can describe the behavior of fluid at the solid boundary by combining the rebound and specular reflection format with a rebound ratio coefficient. The unknown distribution function on the boundary nodes in the BSR scheme (Figure 2) is obtained by

$$f_2(i, 0) = f_4(i, 0)$$
$$f_5(i, 0) = rf_7(i, 0) + (1 - r)f_8(i - 1,0)$$
$$f_6(i, 0) = rf_8(i, 0) + (1 - r)f_7(i + 1,0) \tag{11}$$

where r is the rebound ratio coefficient. $r = 1$ indicates nonslip boundary, $r = 0$ indicates complete slip boundary, and $r = 0.5$ indicates ideal diffuse reflection. In this paper, the above BSR scheme is adopted, and r is equal to 0 and 0.5 to simulate the nonslip boundary and slip boundary.

2.2.3. Numerical Simulation Settings. The scale of the simulation zone is 850 in length and 320 in width. A zone with

length × width = 50 × 320 is set at the left and right sides, respectively, to simulate the injection end and the collecting end of the crack-pore-throat network. The main throats and traffic throats both have an opening of 5. The length of each main throat is 750. The length of each traffic throat is set as 30, 50, 70, ... and 250. The length is also the interval between the two main throats. The crack length is 250, and the opening is 15, 25, 35, and 45. The inlet on the left uses a pressure boundary format, and the outlet on the right uses a fully developed boundary format. The pressure at the two sides is fixed. At the upper and lower boundaries, uniform slip-free boundary or ideal diffuse reflection slip boundary are adopted to simulate the slip and nonslip boundary conditions, respectively.

In the computation, the focus is on the changes of the flux and pressure with geometric parameters, which can help to find the characteristics of the flux distribution between the two main throats and the mechanism to form the water channel.

3. RESULTS AND DISCUSSION

3.1. Model Verification. In order to verify the model, the flow in a tube without slip is simulated first, and then, the numerical results are compared with the analytical solution of the Poiseuille flow. The analytical solution of the speed (u) is as follows

$$u = -\frac{1}{4\mu}\frac{dp}{dx}(b^2 - y^2) \tag{12}$$

where p is the pressure, μ is the viscosity, b is the diameter of the tube, and y is the distance from the center line. The scale of the simulated zone is length × diameter = 500 × 60. The inlet on the left uses a pressure boundary format, and the outlet on the right uses a fully developed boundary format. The Reynolds number is about 7.25. Figure 3 is the comparison of speed distribution in the cross section. The line is the numerical results, and the parabola is the analytical solution. It can be seen that the numerical solution agrees well with the analytical solution.

3.2. Effects of Existence of Crack on Flux. For comparison, the results with no cracks are shown in Figure 4. The total flux is smaller than that with a crack. The development tendency of the flux in the main throats with the interval is similar to that with a crack. The obvious difference is
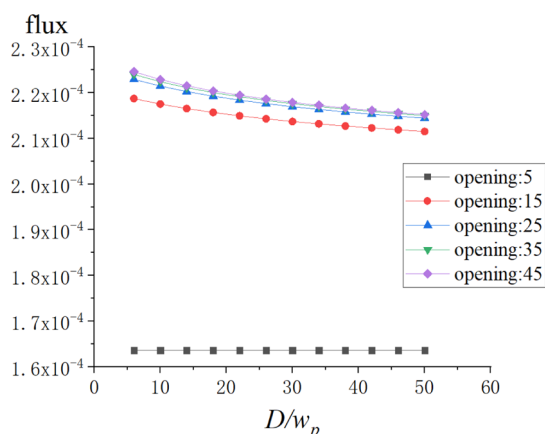
Figure 4. Development of flux with dimensionless interval without cracks.

that the flux in the traffic throats is several orders smaller than that in any main throat. That means, in a uniformly distributed pore-throat network, the fluid will flow mainly in the throats extending parallel to the direction of pressure difference. The flux perpendicular to the direction of pressure difference can be neglected. Therefore, if the throats are paralleled and the distribution is regular, the oil/gas in the throats perpendicular to the direction of pressure difference will not be easily utilized and the displacement efficiency will be very low. It indicates that the irregular crack-throat network is the best choice in the fracking.

3.3. Effects of Inlet Crack on Flux. Figures 5 and 6 show the flux in the throats with dimensionless parameters of w_f/w_p and D/w_p under slip and nonslip boundary conditions, respectively. The crack is set near the inlet. It can be seen that the development trend of the flux is the same under either slip or nonslip boundary conditions, but the flux under slip conditions is greater than that under nonslip boundary conditions. The flux of each throat increases with a smaller and smaller rate with the enlargement of the crack's opening. Under nonslip boundary conditions, with the increase of the parameter D/w_p, the flux of the main throat m_1 (the flux at the outlet of m_1) decreases linearly, while the flux of the main throat m_2 (the flux at the outlet of m_2) decreases slightly first and then increases a little (Figure 5a). However, the flux of m_2

is greater than that of m_1 and the differences enlarge with the increase of the parameter D/w_p. It means that the throat containing a crack has less resistance and larger flux than that without a crack. The increase of D/w_p means the resistance enlargement of the traffic throat. Therefore, the flux exchange between the two main throats decreases. Meanwhile, the throat m_2 has less resistance relative to m_1 because of the existence of the crack, and the flux is surely larger at the same pressure difference.

The positive flux in Figure 5b indicates that the fluid flows from the main throat m_2 to m_1 through the traffic throats t_1, t_2, and t_3, while the negative flux means that the fluid flows from the main throat m_1 to m_2. The flux (absolute value) of the traffic throat t_1 is larger than that of the traffic throats t_2 and t_3. The difference decreases with the increase of parameter D/w_p. The reason is the existence of the crack leads to the increase of flux near the inlet of the throat m_2, and so, the fluid in the throat m_1 is pushed into m_2 fast. With the increase of parameter D/w_p, the fluxes (absolute value) of the traffic throats m_1 and m_2 decrease, while the traffic throat m_1 increases a little. The reduction rate of the flux of throat m_3 becomes smaller with the increase of parameter D/w_p. When D/w_p is greater than 30, the flux of throat m_3 is approximately linear, while it is gradually close to that of m_2 when D/w_p is greater than 40. In other words, the existence of the crack and the changes of the parameter D/w_p affect the flux of each throat/crack greatly.

3.4. Effects of Middle Crack on Flux. Figure 7 and 8 show the relationship between the flux of each throat and the parameter D/w_p and opening when the crack is located in the middle of the throat m_2. The results under slip boundary conditions are shown in Figure 8, while it is under nonslip boundary conditions in Figure 7. With the increase of the parameter D/w_p, the flux of the throat m_1 decreases gradually with a decaying rate, while the flux of the main throat m_2 increases gradually (Figure 8a). They are approximately symmetrical. It can be seen from Figure 8b that the flux of throats t_1 and t_3 is close to each other, but the flow direction is opposite. The fluxes in these two throats decrease with the increase of the parameter D/w_p, and the decreasing rate becomes smaller and smaller gradually. The pressure at the front of the throat m_2 is larger than that of m_1 at the same position, so the fluid flows from m_2 to m_1, while it is, on the
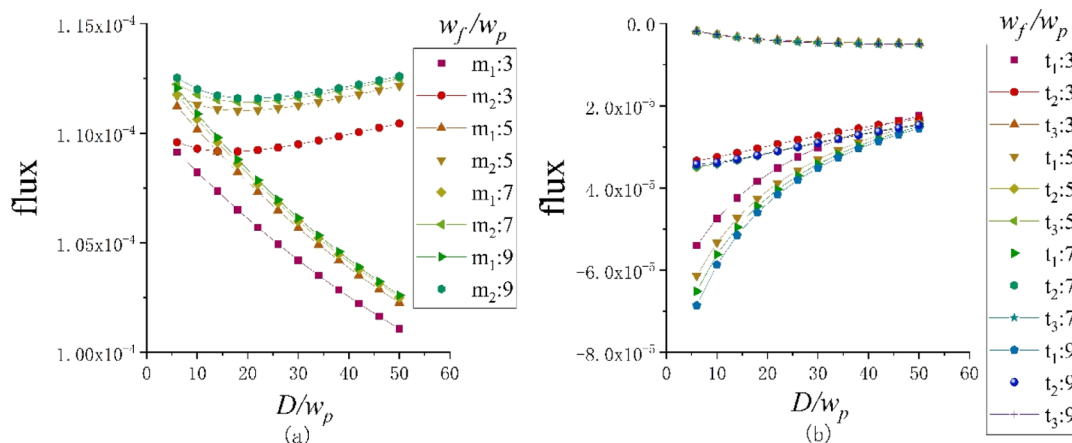

Figure 5. Development of flux of each throat with D/w_p and opening under nonslip condition. The crack is near the inlet. (a) Flux of the two main throats and (b) flux of the three traffic throats. The flow rate at the end of each throat is named the flux of this throat.
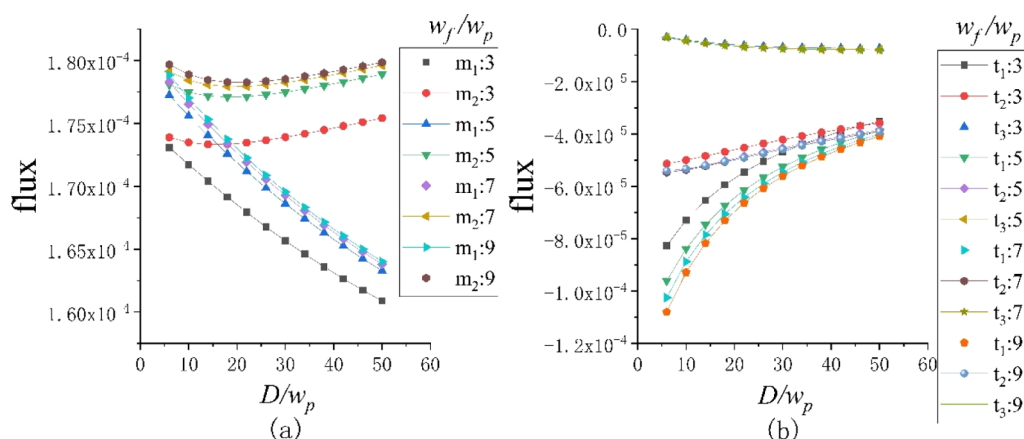
Figure 6. Relationship between the flux and the parameter D/w_p under slip conditions. The crack is near the inlet with different opening. (a) Flux of main throats versus D and (b) flux of traffic throats versus D.
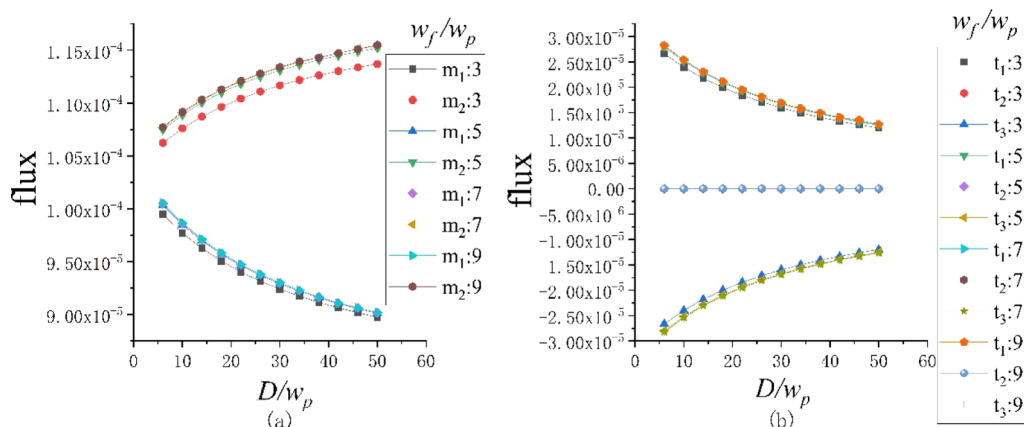

Figure 7. Development of flux of each throat with D/w_p and opening under no-slip condition. The crack is located in the middle of throat m_1. (a) Flux of the main throat and (b) flux of the traffic throat.
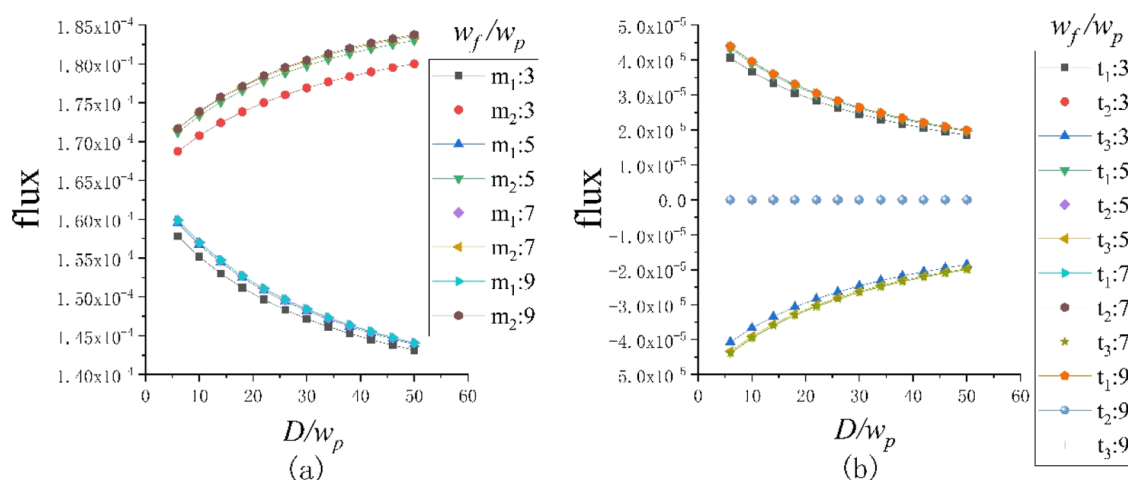

Figure 8. Changes of flux with D/w_p and opening under slip conditions. The crack is located in the middle of the throat m_2. (a) Flux of the main throats and (b) flux of the traffic throats.

contrary, at t_3 when the crack is in the middle. Meanwhile, the throat-crack system is symmetrical around the crack center in this case, so the flow directions are opposite, similar to that of m_1 and m_2. The flux of each throat increases in a smaller rate with the increase of the crack's opening. Compared with the results with the crack near the inlet, the existence of the crack

enhances the flow of the throat m_2 obviously. If more fluid is sucked into the throat with crack, the water channel may form.

3.5. Effects of Outlet Crack on Flux. Figures 9 and 10 show the relationship between the flux of each throat and the parameter D/w_p and crack opening when the crack is located near the outlet. The results in Figure 9 are computed under the nonslip boundary condition, while in Figure 10, the results are
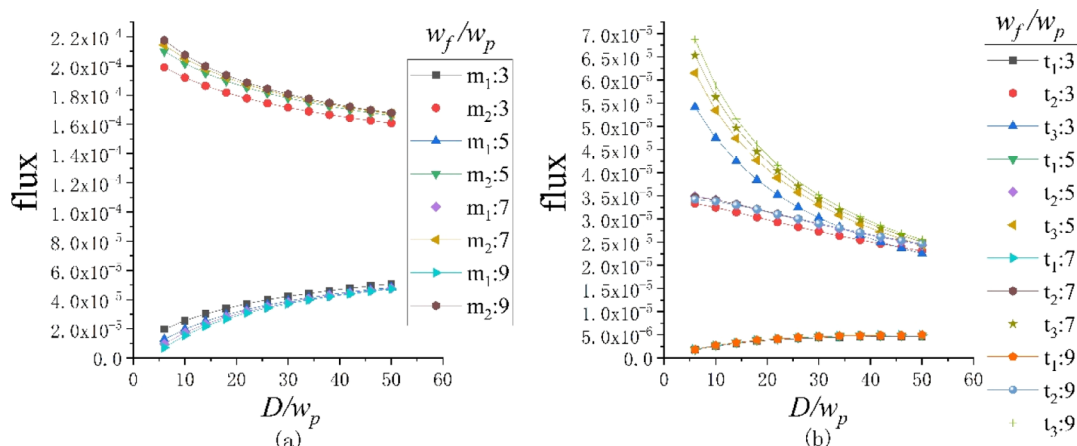
Figure 9. Development of flux of each throat with D/w_p and opening under nonslip conditions when the crack is located near the outlet. (a) Flux of the main throats and (b) flux of the traffic throats.
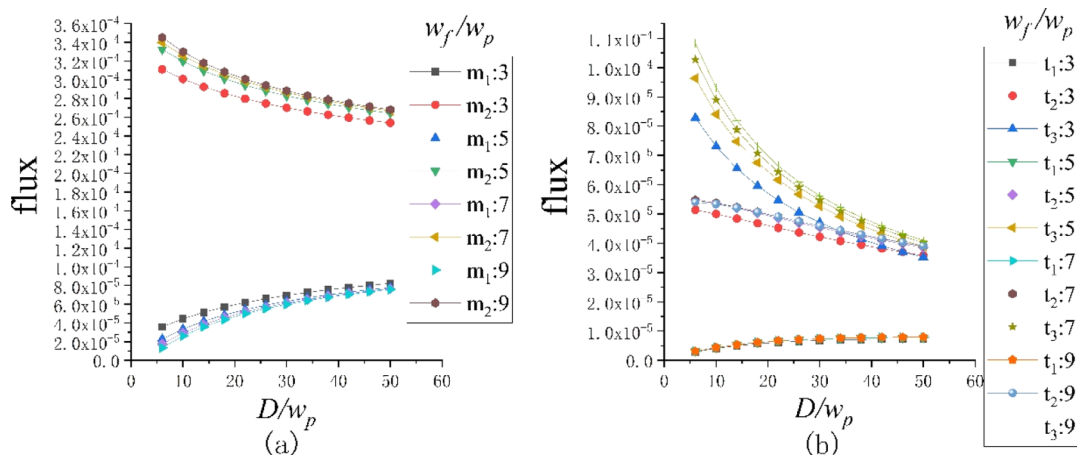

Figure 10. Development of flux of each throat with D/w_p and opening under slip conditions when the crack is located near the outlet. (a) Flux of the main throat and (b) flux of the traffic throat.

computed under the slip boundary condition. The flux of the throat m_1 increases gradually with D/w_p while that of m_2 decreases gradually. The flux of m_2 is about 10 times (Figure 9) than that of m_1 at nonslip boundary conditions and about 20 times (Figure 10) at slip boundary conditions. The difference expands with the increase of D/w_p. Nevertheless, the flux of the throat m_2 is much larger than that when the crack is near the inlet and in the middle. So it is more possible to promote the formation of the water channel when the crack is located near the outlet.

The flux of the traffic throat t_1 increases gradually and is one order smaller than that of t_2 and t_3. The flux of t_2 decreases linearly and slowly. The flux of t_3 drops rapidly at first and then slowly with the increase of D/w_p. In the case of $D/w_p > 4$, the flux of m_3 is very close to that of m_2. The flux curves of m_1 and m_2 are approximately symmetrical about a horizontal axis. The results show that the effects of the crack are the largest when it is near the outlet in the three cases.

3.6. Effects of Nonslip and Slip Boundary on Flux. The numerical results show that the slip boundary condition only enlarges the flux but does not affect the distribution form of the velocity. The reason is that the slip boundary leads to the decrease of the resistance, for example, more fluid is rebound to the flow. It can be seen from the Poiseuille flow (eq 12).

As shown in Figure 11, distribution of the velocity is similar at different rebound coefficients, for example, the slip degree on the boundary. Only the value changes with the rebound coefficient. The lowest curve is the result with nonslip boundary, corresponding to the Poiseuille flow. The curve of
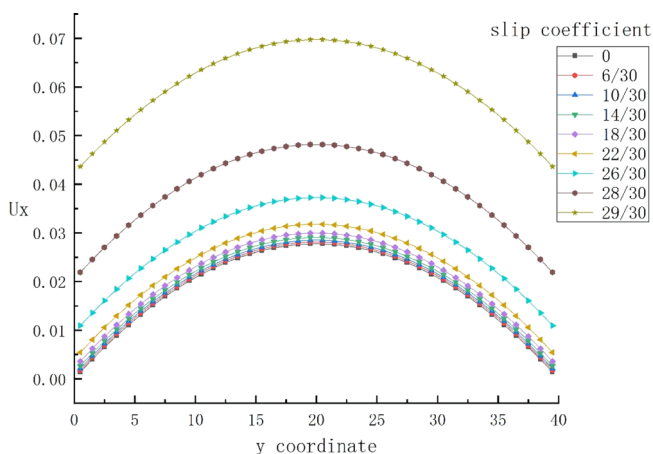

Figure 11. Sectional velocity distribution between two-dimensional infinitely long parallel plates under different slip coefficients.
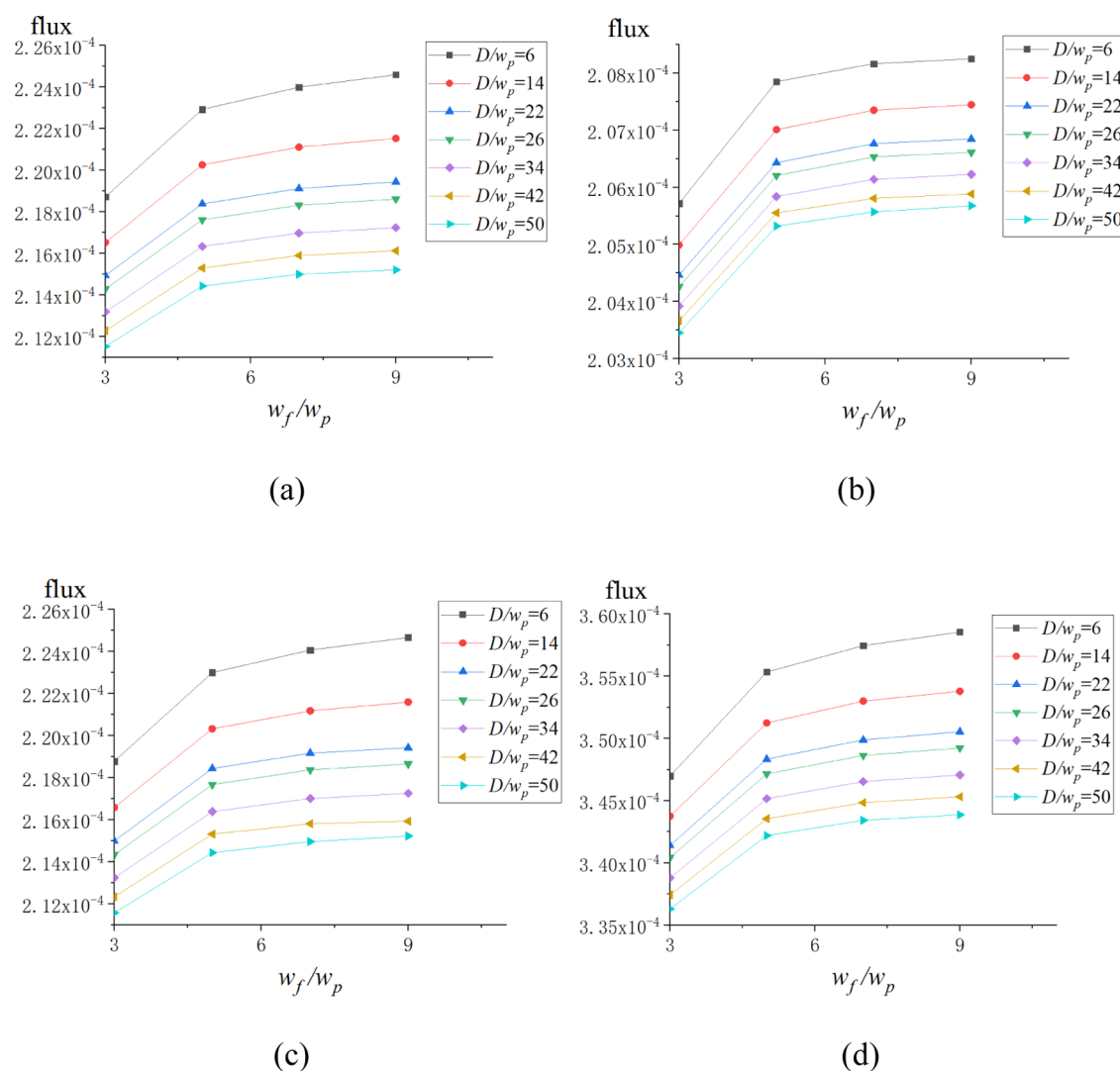
Figure 12. Relationship between the total flux of the two main throats and the opening ratio of crack-to-throat (w_f/w_p). The flow under three positions of the crack is computed. (a–c) Results with nonslip boundary conditions and (d) results with slip boundary conditions. (a) The crack is located near the inlet with nonslip boundary; (b) The crack is located in the middle with nonslip boundary; (c) The crack is located near the outlet with nonslip boundary; (d) The crack is located near the inlet with slip boundary.

the velocity distribution moves upward with the increase of the rebound coefficient. The total flux under the slip boundary condition approximated equals the accumulation of the viscous flow and the slip flow.

Figure 12 shows the relationship between the total flux of the main throats and the opening ratio of crack-to-throat (w_f/w_p) when the crack is located at different positions. The curves in Figure 12a–c are computed with nonslip boundary. The curves in Figure 12d are the result with slip boundary. It can be seen that the total flux increases with the parameter w_f/w_p. The total flux changes very little when w_f/w_p is over about 9. The flux ratio of the crack-to-throat is the biquadrate of w_f/w_p at the same length and pressure gradient, so the changes of flux in the throats connected with the crack is smaller and also smaller when w_f/w_p is over some value. The curve when the crack is near the inlet is very close to that near the outlet. The total flux under slip boundary conditions is about 1.5 times than that of under nonslip boundary conditions.

The development of the flux in each throat has been illustrated in the above sections. The total flux is discussed in this section. Figure 13 shows the changes of the total flux (the

sum of the flux of the two main throats) with the parameter D/w_p. The total flux decreases with the enlargement of the parameter D/w_p, and the decrease rate becomes smaller and smaller under either slip or nonslip boundary conditions. With the increase of rebound coefficient, the flux increases.

Figure 13 shows the development of the total flux with the locations of the crack. No matter where the crack is located, the total flux always increases with the increase of the crack opening, but the increasing extent decreases as the crack opening increases. The total flux with slip boundary is greater than that with nonslip boundary. It is almost equal to each other when the crack is near the inlet and near the outlet, while greater than that in the middle. However, the flux ratio of the throat m_2 to m_1 with the crack near the outlet is the largest in the three locations. That means, the crack should be prevented to form near the outlet during fracking or oil/gas displacement. Otherwise the water/gas channel can occur.

3.7. Effects of Geometric Parameters on Flux. To observe the effects of the geometric parameters on the flux of the two main throats, the flux ratio of the throat m_1 to m_2 is shown in Figure 14. Only the results under nonslip boundary
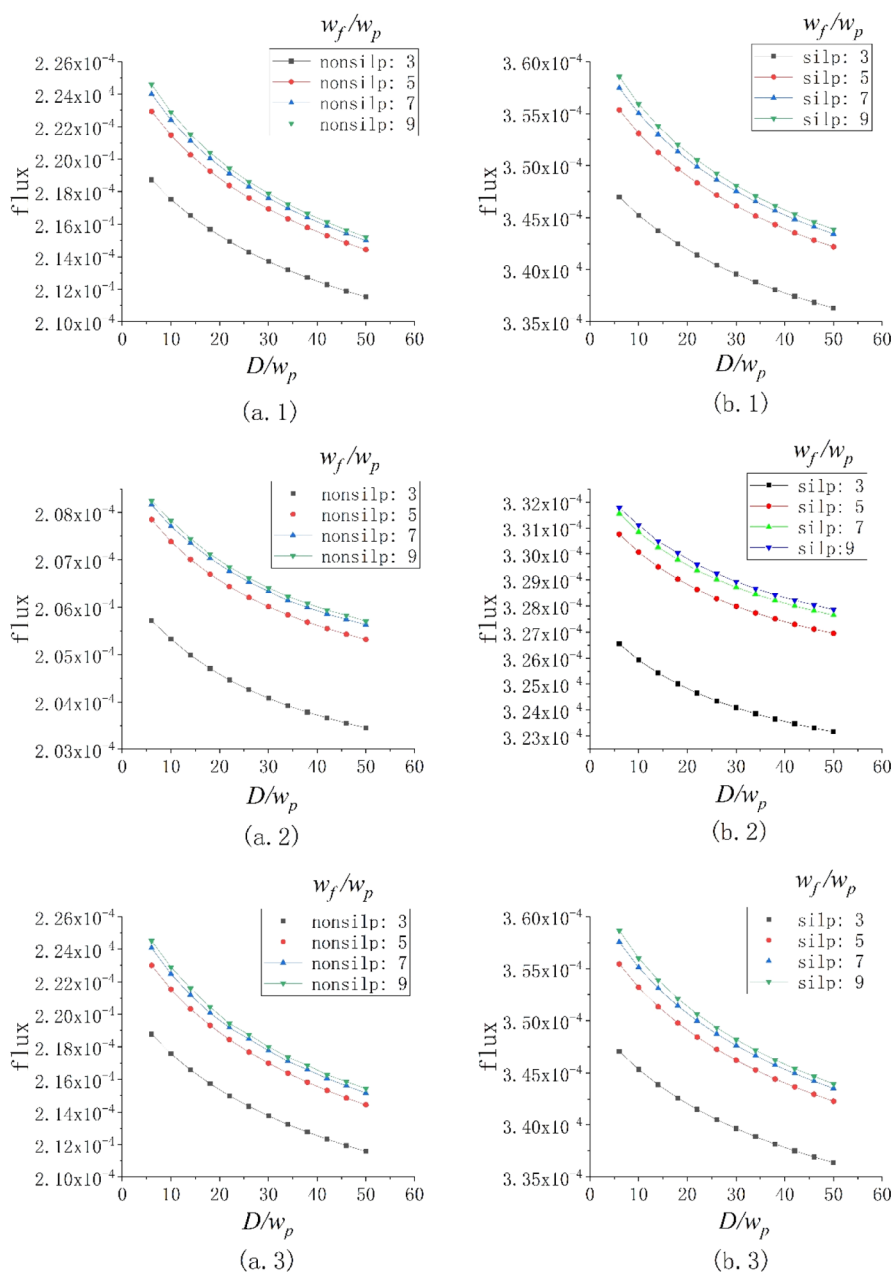
Figure 13. Relationship between the total flux with different crack positions and the parameter D/w_p. (a.1~a.3) Results of nonslip boundary and (b.1~b.3) results of slip boundary.

conditions are given here. The effects of the interval are considered. It can be seen that the flux ratio when the crack is near the inlet is very close to that when the crack is located in the middle and the values are large (over 0.75 in the parameter zones adopted in this paper) and decreases with the rise of the interval. That means, the flux in the two main throats are very close to each other in the two cases and so the water channel does not tend to occur. The flux ratio when the crack is located near the outlet is smaller than that in the other two cases, and the values increase with the rise of the interval. It indicates that the water channel is more possible to occur when the cracks are located near the outlet although the total flux is almost equal to that when the crack is located near the inlet.

4. CONCLUSIONS

Based on an idealized crack-pore-throat network model, the influence of geometric parameters, including the opening ratio of crack-to-throat and dimensionless interval between the two main throats, on the flow is studied by the LBM method. The main results are as follows:

1. The flux and the value of velocity increase but the form of the velocity distribution along intersection does not change under slip boundary conditions relative to that under nonslip boundary conditions.
2. The total flux when the crack near inlet is nearly equal to that near outlet but larger than that in the middle. The flux of the main throat containing the crack is the largest when the crack is near the outlet. That means, the water channel is the largest possible to form when the crack is located near the outlet.
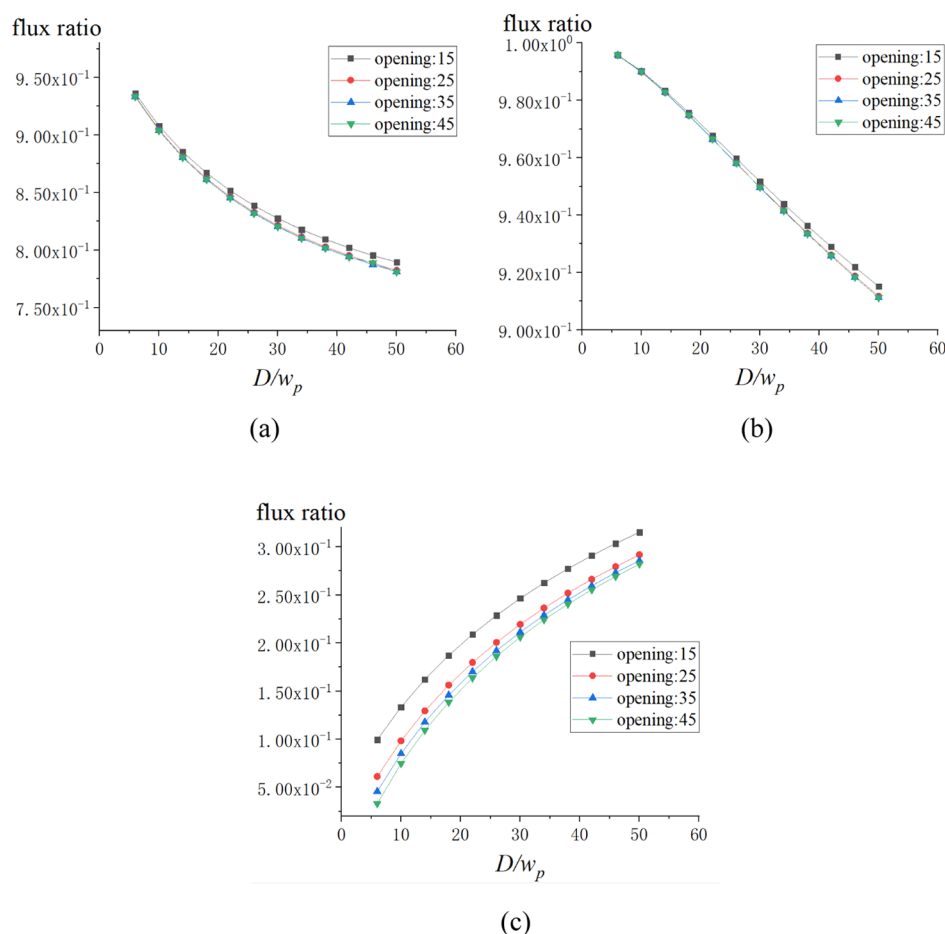
Figure 14. Flux ratio of the two main throats (flux of m_1/flux of m_2).(a) The crack is located near the inlet; (b) The crack is located in the middle; (c) The crack is located near the outlet.

3. The increase in the opening ratio of crack-to-throat enlarges the total flux. The increase speed decreases gradually. The total flux changes very little when w_f/w_p is over about 9.0.

4. When the pore size is too small to ignore the Klinberg effect, among the factors w_f/w_p, D/w_p, and nonslip/slip boundary conditions, the degree of slip is the most important factor affecting the total flux and the value of velocity.

5. In a regular throat-pore network model which consisted of only horizontal and vertical distributed throats with the same sizes, the flux in the main throats are nearly equal. The flux in the traffic throats can be neglected. Obviously, this is caused by the very small pressure difference at both ends of the traffic throat. This also means that if there is another liquid in the traffic throat, it will be difficult to drive out the liquid because the pressure difference between its two ends is too small. That means, in such a network, the oil/gas in the traffic throats is difficult to be displaced.

AUTHOR INFORMATION

Corresponding Author

Yingjun Li − *State Key Laboratory for Geomechanics and Deep Underground Engineering, China University of Mining and Technology (Beijing), Beijing 100083, China;* Email: lyj@aphy.iphy.ac.cn

Authors

Li Lu − *State Key Laboratory for Geomechanics and Deep Underground Engineering, China University of Mining and Technology (Beijing), Beijing 100083, China;* ◉ orcid.org/ 0000-0003-2105-1352

Xuhui Zhang − *Institute of Mechanics, Chinese Academy of Sciences, University of Chinese Academy of Sciences, Beijing 100190, China*

Complete contact information is available at: https://pubs.acs.org/10.1021/acsomega.0c05113

Notes

The authors declare no competing financial interest.

ACKNOWLEDGMENTS

REFERENCES

(1) Liu, H.; Zhang, X.; Lu, X.; Liu, Q. Study on flow in fractured porous media using pore-fracture network modeling. *Energies* **2017**, *10*, 1984.

(2) Cui, J.; Cheng, L.; Li, L. Apparent permeability and representative size of shale: a numerical study on the effects of organic matter. *Comput. Geosci.* **2018**, *22*, 1083−1091.

(3) Cui, J. Oil transport in shale nanopores and micro-fractures: Modeling and analysis. *J. Pet. Sci. Eng.* **2019**, *178*, 640−648.

(4) Yang, L.; Zhang, X.; Zhou, T.; Lu, X.; Zhang, C.; Zhang, K. The effects of ion diffusion on imbibition oil recovery in salt-rich shale oil reservoirs. *J. Geophys. Eng.* **2019**, *16*, 525−540.

(5) Yang, L.; Ge, H.; Shi, X.; Cheng, Y.; Zhang, K.; Chen, H.; Shen, Y.; Zhang, J.; Qu, X. The effect of microstructure and rock mineralogy on water imbibition characteristics in tight reservoirs. *J. Nat. Gas Sci. Eng.* **2016**, *34*, 1461−1471.

(6) Wang, D.; Dong, Y.; Sun, D.; Yu, B. A three-dimensional numerical study of hydraulic fracturing with degradable diverting materials via CZM-based FEM. *Eng. Fract. Mech.* **2020**, *237*, 107251.

(7) Liu, R.; Jiang, Y.; Huang, N.; Sugimoto, S. Hydraulic properties of 3D crossed rock fractures by considering anisotropic aperture distributions. *Adv. Geo-Energy Res.* **2018**, *2*, 113−121.

(8) Wang, D.; Zhou, F.; Dong, Y.; Sun, D.; Yu, B. Experimental investigation of thermal effect on fracability index of geothermal reservoirs. *Nat. Resour. Res.* **2020**, 1−16.

(9) Wang, D.; Bian, X.; Qin, H.; Sun, D.; Yu, B. Experimental Investigation of Mechanical Properties and Failure Behavior of Fluid-Saturated Hot Dry Rocks. *Nat. Resour. Res.* **2020**, 1−17.

(10) Meng, M.; Ge, H.; Shen, Y.; Hu, Q.; Li, L.; Gao, Z.; Tian, T.; Chao, J. The effect of clay-swelling induced cracks on imbibition behavior of marine shale reservoirs. *J. Nat. Gas Sci. Eng.* **2020**, *83*, 103525.

(11) Meng, M.; Ge, H.; Shen, Y.; Li, L.; Tian, T.; Chao, J. The effect of clay-swelling induced cracks on shale permeability during liquid imbibition and diffusion. *J. Nat. Gas Sci. Eng.* **2020**, *83*, 103514.

(12) Liu, Y.; Gao, D.; Li, Q.; Wan, Y.; Duan, W.; Zeng, X.; Lu, X. Mechanical frontiers in shale-gas development. *Adv. Mech.* **2019**, *49*, 201901.

(13) Darabi, H.; Ettehad, A.; Javadpour, F.; Sepehrnoori, K. Gas flow in ultra-tight shale strata. *J. Fluid Mech.* **2012**, *710*, 641.

(14) Wang, P.; Zhang, X.; Lu, X.; Zheng, W.; Liu, Q. A dual percolation model for predicting the connectivity of fractured porous media. *Water Resour.* **2016**, *43*, 95−110.

(15) Deng, S.. On the Mechanism of Flow through Dual Media: Pore-Fracture Network Modeling and Experimental Study. Dissertation for Master Degree, University of Chinese Academy of Sciences, 2014.

(16) Kang, Q.; Lichtner, P. C.; Zhang, D. Lattice Boltzmann pore-scale model for multicomponent reactive transport in porous media. *J. Geophys. Res. B Solid Earth Planets* **2006**, *111*, B05203.

(17) Fathi, E.; Tinni, A.; Akkutlu, I. Y. Shale gas correction to Klinkenberg slip theory. In *SPE Americas Unconventional Resources Conference*, 2012, January.

(18) Fathi, E.; Akkutlu, I. Y. Lattice Boltzmann method for simulation of shale gas transport in kerogen. *SPE J.* **2012**, *18*, 27−37.

(19) Ning, Z.; Wang, B.; Yang, F.; Zeng, Y.; Chen, J.; Zhang, L. Microscale effect of microvadose in shale reservoirs. *Petrol. Explor. Dev.* **2014**, *41*, 492−499.

(20) Ning, Y.; Jiang, Y.; Liu, H.; Qin, G. Numerical modeling of slippage and adsorption effects on gas transport in shale formations using the lattice Boltzmann method. *J. Nat. Gas Sci. Eng.* **2015**, *26*, 345−355.

(21) Benamram, Z.; Tarakanov, A.; Nasrabadi, H.; Gildin, E. Efficient Fractured Reservoir Simulation Using Lattice Boltzmann Method. In *SPE Latin American and Caribbean Petroleum Engineering Conference*, 2015, November.

(22) Wang, Z.; Guo, Y.; Wang, M. Permeability of high-Kn real gas flow in shale and production prediction by pore-scale modeling. *J. Nat. Gas Sci. Eng.* **2016**, *28*, 328−337.

(23) Moghaddam, R. N.; Jamiolahmady, M. Study of slip flow in unconventional shale rocks using lattice Boltzmann method: Effects of boundary conditions and TMAC. *Transp. Porous Media* **2017**, *120*, 115−139.

(24) Li, X.; Fan, J.; Yu, H.; Zhu, Y.; Wu, H. Lattice Boltzmann method simulations about shale gas flow in contracting nano-channels. *Int. J. Heat Mass Transfer* **2018**, *122*, 1210−1221.

(25) Shan, X.; Chen, H. Lattice Boltzmann model for simulating flows with multiple phases and components. *Phys. Rev. E: Stat. Phys., Plasmas, Fluids, Relat. Interdisc. Top.* **1993**, *47*, 1815.

(26) Lallemand, P.; Luo, L.-S. Theory of the lattice Boltzmann method: Dispersion, dissipation, isotropy, Galilean invariance, and stability. *Phys. Rev. E: Stat. Phys., Plasmas, Fluids, Relat. Interdisc. Top.* **2000**, *61*, 6546.

(27) d'Humières, D.; Shizgal, B. D. *Rarefied gas dynamics: theory and simulations*; The American Institute of Aeronautics and Astronautics, 1992, pp 450−458.

(28) Bhatnagar, P. L.; Gross, E. P.; Krook, M. A model for collision processes in gases. I. Small amplitude processes in charged and neutral one-component systems. *Phys. Rev.* **1954**, *94*, 511.

(29) Chen, S.; Chen, H.; Martnez, D.; Matthaeus, W. Lattice Boltzmann model for simulation of magnetohydrodynamics. *Phys. Rev. Lett.* **1991**, *67*, 3776.

(30) Qian, Y. H. *Lattice gas and lattice kinetic theory applied to the Navier-Stokes equations*; Doktorarbeit, Universite Pierre et Marie Curie, Paris, 1990.

(31) Leclaire, S.; Reggio, M.; Trépanier, J.-Y. Numerical evaluation of two recoloring operators for an immiscible two-phase flow lattice Boltzmann model. *Appl. Math. Model.* **2012**, *36*, 2237−2252.

(32) Ziegler, D. P. Boundary conditions for lattice Boltzmann simulations. *J. Stat. Phys.* **1993**, *71*, 1171−1177.